Research Square

Preprints are preliminary reports that have not undergone peer review. They should not be considered conclusive, used to inform clinical practice, or referenced by the media as validated information.

# Development of Schiff Base Chemosensors for Visual Detection of $Cu^{2+}$, $Fe^{2+}$, and $Pb^{2+}$ Ions: Experimental Validation and Theoretical Support

**Swathi Harithas**
Presidency University
**Chaitanya Lakshmi G**
CHAITANYALAKSHMIG@PRESIDENCYUNIVERSITY.IN

Presidency University

**Research Article**

**Keywords:** Chemosensor, Schiff bases, Metal ions, Colorimetric detection, DFT studies

**Posted Date:** October 16th, 2026

**DOI:** https://doi.org/10.21203/rs.3.rs-10956349/v1

**License:** This work is licensed under a Creative Commons Attribution 4.0 International License. Read Full License

**Additional Declarations:** No competing interests reported.

# Development of Schiff Base Chemosensors for Visual Detection of $Cu^{2+}$, $Fe^{2+}$, and $Pb^{2+}$ Ions: Experimental Validation and Theoretical Support

Swathi Harithas[1], Chaitanya Lakshmi G[2]

[1]Department of chemistry, Presidency University, Bengaluru INDIA

Corresponding Author Mail Id: chaitanyalakshmig@presidencyuniversity.in

**Abstract:**

The design and development of selective chemosensors for toxic metal ions remain of significant importance due to their environmental and biological impact. In this study, a series of Thiocarbohydrazide-based Schiff base ligands (TS, TC, and TV) were synthesized and characterized, with a focus on their Azomethine (-C=N–) moieties capable of coordinating with transition metal ions. The sensing performance of the ligands was evaluated toward $Cu^{2+}$, $Fe^{2+}$, and $Pb^{2+}$ ions using a simple colorimetric monitoring approach in a mixed aqueous–ethanol medium. Upon addition of metal ions, the ligands exhibited distinct and easily discernible color changes, allowing for straightforward visual identification. UV–Visible absorption studies verified the formation of the complexes, while Job's plot analysis consistently demonstrated a 1:1 metal-to-ligand binding stoichiometry in all cases. Theoretical evaluations based on Conceptual Density Functional Theory (CDFT) were undertaken to complement the experimental findings. Several global reactivity descriptors, including electronegativity, HOMO–LUMO energy gap, molecular hardness, softness, and dipole moment, were calculated to provide insights into the electronic structure and binding tendencies of the ligands. These results supported the proposed bidentate coordination mode through the Azomethine nitrogen atoms, which facilitates stable complex formation. Overall, the combination of experimental and theoretical investigations highlights the potential of these Schiff base ligands as efficient and selective chemosensors for $Cu^{2+}$, $Fe^{2+}$, and $Pb^{2+}$ ions. Their sensitivity, simple detection mechanism, and strong coordination behaviour emphasize their applicability in analytical sensing and environmental monitoring.

**Keywords**: Chemosensor, Schiff bases, Metal ions, Colorimetric detection; DFT studies.

## 1. Introduction.

Since they can stabilise a wide range of metal ions and have structural flexibility that makes them adaptable to donor sites, schiff base ligands have been the center of attention in coordination chemistry [1]. Schiff bases are often created by condensing primary amines with carbonyl compounds. What makes them unique is the presence of the azomethine (>C=N-) functional group, which is crucial for metal binding [2]. Their excellent chelating ability, variable electrical properties, and ease of production make them very desirable for applications in chemical sensing, biological systems, materials research, and catalysis [3]. In particular, thiocarbohydrazide-based Schiff base ligands are intriguing due to their ability to function as efficient multidentate chelators, thanks to their increased binding affinity and number of donor sites [4].

Thiocarbohydrazide is a sulfur-and nitrogen-rich precursor with many metal-ion-binding donor sites. When added to Schiff base frameworks, thiocarbohydrazide increases their chelation potential, which often leads to the formation of stable multidentate complexes. These ligands can coordinate through sulphur and nitrogen donor atoms, which improves their affinity and selectivity for heavy and transition metals [5]. Schiff bases based on thiocarbohydrazide are attractive choices for designing functional coordination molecules with targeted reactivity and sensing capabilities because of this property [6]. Thiocarbohydrazide units enhance the complexes' stability and selectivity by providing additional donor sites for multidentate coordination, which in turn increases their binding affinity [7].

The three primary metal ions that need to be considered are lead ($Pb^{2+}$), copper ($Cu^{2+}$), and iron ($Fe^{2+}$). Trace metals copper and iron are essential for enzyme activity, oxygen transport, and metabolic pathways; nevertheless, an imbalance or excess of these metals is associated with oxidative stress and diseases such dementia and organ failure. [8]. In contrast, lead is completely useless to biology and causes developmental and neurological problems at trace levels. Therefore, it is crucial to identify and monitor these ions in biological and environmental contexts [9].

In light of the foregoing, we provide here the synthesis and characterisation of three Schiff base ligands (TS, TC, and TV) based on thiocarbohydrazide and assess their capacities as colorimetric chemosensors for $Cu^{2+}$, $Fe^{2+}$, and $Pb^{2+}$ ions. To determine binding stoichiometry, we used colorimetric monitoring, UV-Visible spectroscopy, and Job's plot analysis to evaluate the sensing capability of these ligands. In addition, CDFT-based theoretical studies were carried out to delve more into their electrical characteristics, reactivity, and binding processes. The combination of theoretical and experimental approaches reveals that these ligands have great promise as efficient and selective chemosensors, which could have far-reaching consequences for analytical and ecological fields.

## 2. Experimental section.

### *2.1. Materials and methodology.*

No additional purification was performed on any of the chemicals before use; they were all acquired from commercial vendors in analytical research grade. Procurement of salicylaldehyde, cinnamaldehyde, vanillin, lead(II) acetate trihydrate, ferrous (II) sulphate heptahydrate, and copper(II) sulphate pentahydrate was done by TCI Co., Ltd. Ethanol and dimethylformamide (DMF) were supplied by SRL. The Supplemental Information (SI) contains comprehensive experimental protocols.
The melting points were recorded uncorrected from data collected using an electro thermal equipment with open capillary tubes. A JEOL NMR 400MHz (JNM-ECZL400S) in DMSO-$d_6$ was used to record proton ($^1H$) and $^{13}C$ NMR spectra, with tetramethylsilane (TMS) serving as the internal reference. A mass analyser called an LC-MS 2010 SHIMADZU was used to get the LC-MS spectra. The Bruker Alpha-T FTIR spectrophotometer was used to gather infrared spectra (KBr) in the 4000-400 $cm^{-1}$ range, while a Shimadzu model 1650 double-beam spectrophotometer was used to measure UV-visible electronic spectra in the 200-800 nm range, with ethanol as the solvent. A PerkinElmer 2400 CHNS analyser was used to measure the amounts of carbon, hydrogen, sulphur, and nitrogen in the sample.

*2.2 Synthesis of the Chemosensors.*

*2.1.1. Synthesis of 1,2,4-Triazole and Its Schiff Base Derivatives.*

The reaction of 10 grams of thiocarbohydrazide with 60 millilitres of glacial acetic acid was stirred continuously for four to six hours. After it cooled, 1,2,4-triazole solidified into a white substance that could be filtered out and recrystallised [10]. In an Erlenmeyer flask, 1,2,4-triazole (1 mmol) and a number of aromatic aldehydes (1 mmol each), including salicylaldehyde, cinnamonaldehyde, and vanillin, were mixed in 25 mL of ethanol and agitated for around four hours. We filtered the resulting coloured precipitate, rinsed it with hot methanol, and then let it air dry. Recrystallisation from ethanol was used for final purification, resulting in coloured crystalline solids. Schema 1-3 shows the synthetic route for the different Schiff base derivatives, and Table 1 summarises their physical properties and yields.

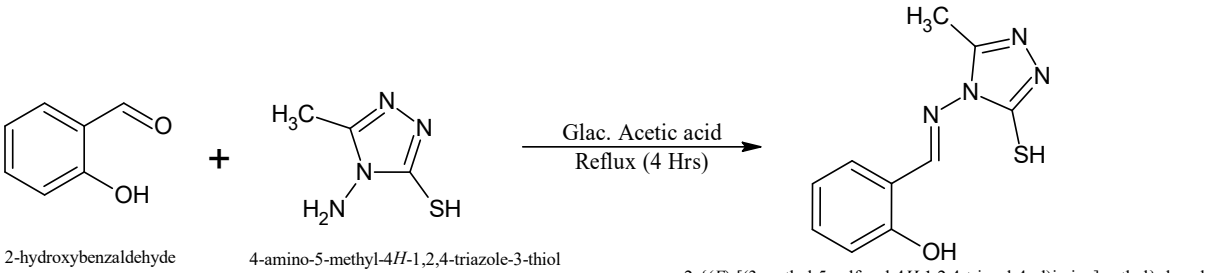


**Scheme-1**: Synthetic route to TS

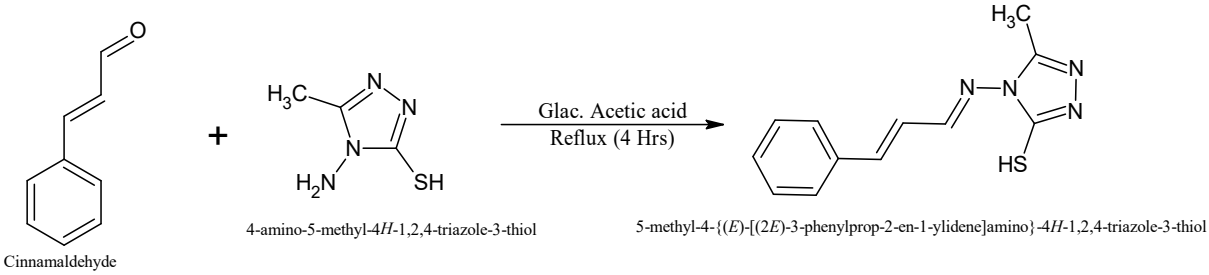


**Scheme-2**: Synthetic route to TC

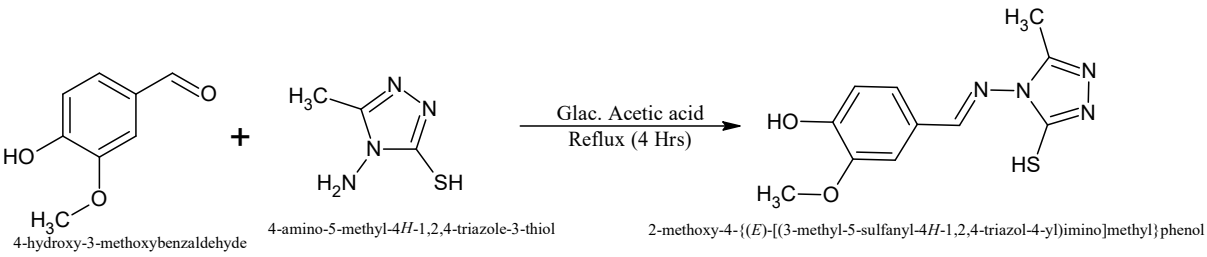


**Scheme 3**: Synthetic route to TV

*2.1.2. Preparation of colorimetric working Solution*

To prepare 1 × $10^{-2}$ M stock solutions of transition metal ions, the respective salts of metal ions were dissolved in deionized water and stored in tightly closed containers. Schiff base ligands (TS, TC, and TV) were dissolved in ethanol to prepare 1 × $10^{-2}$ M stock solutions. The ligands exhibited excellent solubility in ethanol, which is completely miscible with water, ensuring homogeneous mixing with aqueous metal ion solutions during subsequent analytical procedures. (**Scheme-4**)

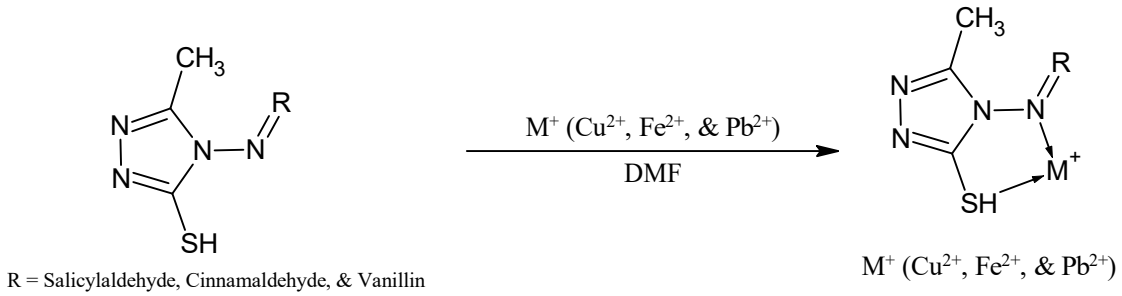


**Scheme 4**: Represntation of Metal-ligand interaction

*2.3. Theoretical studies.*

The synthesised Schiff bases' sensing behaviour was further studied by utilising Density Functional Theory (DFT) simulations to examine their structural and electrical features. We performed all of our calculations using the software application Gaussian 09 [11]. A combination of the B3LYP functional and the 3-21G basis set was used to optimise the molecular geometries [12]**.**

*2.4. Colorimetric Sensing study.*

*2.4.1. Electronic Absorption Spectral Analysis.*

To conduct colorimetric sensing studies, 1 mL of metal ion stock solution (1.0 × $10^{-2}$ M) was combined with 1 mL of Schiff base ligand stock solution (1.0 × $10^{-2}$ M) in a 10 mL volumetric flask [13]. The combination was diluted to the specified level with ethanol, and the pH was adjusted to basic medium. After full mixing at ambient temperature, the resultant solution was exposed to UV-Vis spectroscopy to monitor changes in absorption spectra caused by complex formation [14].

## 3. Results and Discussion.

Isolated as highly coloured crystalline solids, the synthesised Schiff base ligands showed no signs of degradation when exposed to room temperature and humidity. They were suitable for additional spectroscopic investigations and had a good solubility profile since they dissolved easily in a variety of organic solvents including ethanol, chloroform, DMF, and DMSO. The suggested molecular compositions were confirmed by the elemental analysis findings, which were highly concordant with the computed values. The key physical and analytical parameters of the ligands are summarized in **Table-1 and** the EDAX results are presented in Fig-1**.**

**Table-1.** Physico-chemical characteristics, Elemental analytical data of chemosensors.

| Species | Molecular formula | Color | Mlr. Wt. | Yield (%) | MP ($^{O}C$) | Elemental analysis Calculated (analyzed) | | | | |
|---|---|---|---|---|---|---|---|---|---|---|
| | | | | | | C | H | O | N | S |
| TC | $C_{12}H_{12}N_4S$ | Brown | 244.31 | 65 | 111 | 58.94 (57.98) | 4.91 (4.03) | -- -- | 22.92 (22.73) | 13.12 (12.96) |
| TS | $C_{10}H_{10}N_4OS$ | Reddish brown | 234.27 | 63 | 121 | 51.22 (50.93) | 4.26 (4.10) | 6.82 (6.43) | 23.90 (23.47) | 13.68 (13.09) |
| TV | $C_{11}H_{12}N_4O_2S$ | Green | 264.30 | 70 | 90 | 49.94 (49.08) | 4.54 (4.08) | 12.10 (11.98) | 21.18 (21.09) | 12.13 (12.09) |

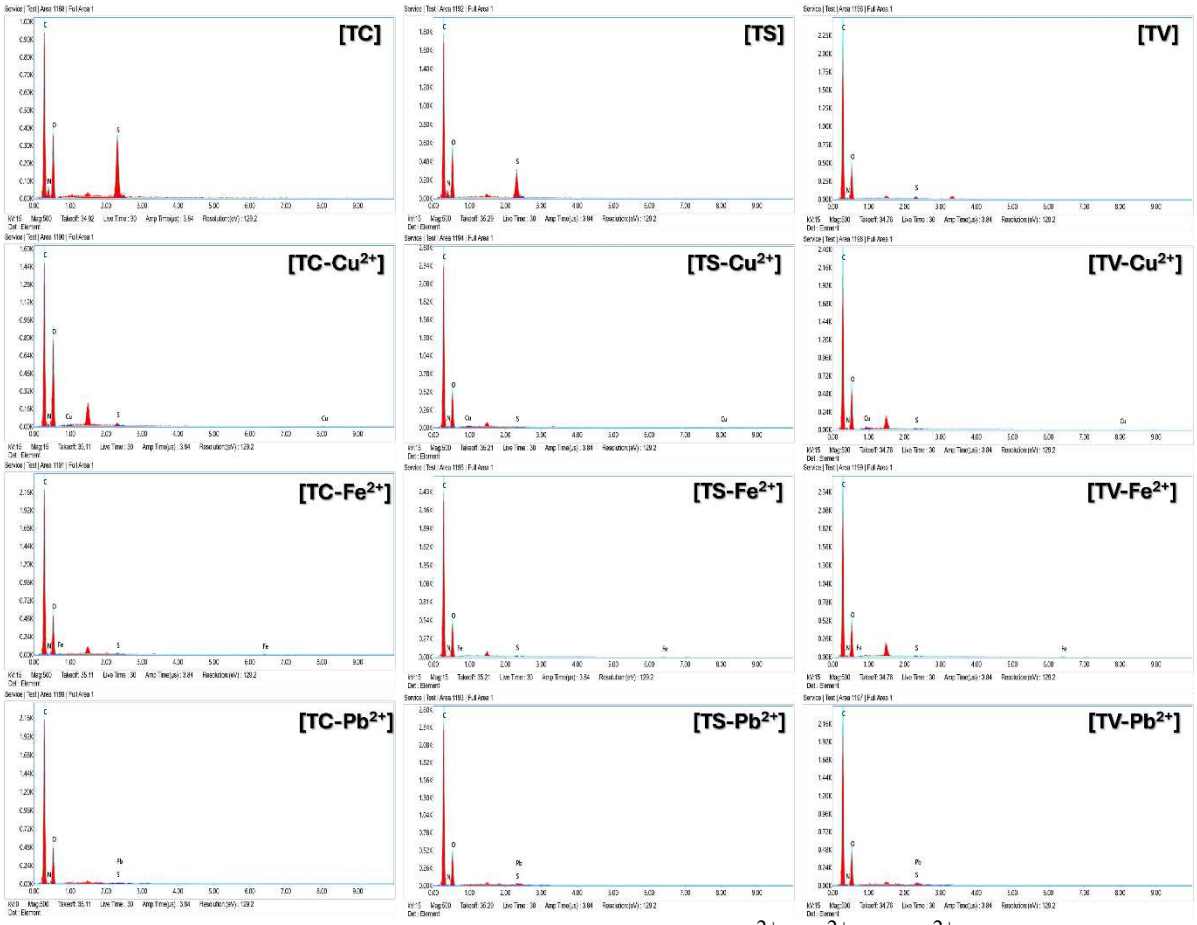


**Fig-1:** EDAX data of the TC, TS, and TV with $Cu^{2+}$, $Fe^{2+}$, & $Pb^{2+}$ metal ions.

### *3.1. Synthesis and Characterization.*

#### *3.1.1. $^{1}H$ and $^{13}C$ NMR spectral analysis.*

$^{1}H$ and $^{13}C$ NMR spectra were recorded in DMSO-$d_6$ at 400 MHz ($^{1}H$) and 100 MHz ($^{13}C$) on a JEOL NMR 400MHz (JNM-ECZL400S) spectrometer. Chemical shifts (δ) are reported in ppm relative to TMS as an internal reference. The interpreted NMR values are summarized in **Table-2**.

**Table-2:** The interpreted NMR data of the Schiff base ligand.

| | Ligand | δ (ppm) | Integration | Multiplicity | Assignment | Group/Moiety |
|---|---|---|---|---|---|---|
| **$^{1}$H** | TC | 11.104 | 1H | S | -SH | -SH proton of 1,2,4-triazole moiety.[15] |
| | | 8.957 | 1H | S | -C=N- | Azomethine proton (Schiff base linkage) [16] |
| | | 7.662-6.908 | 7H | M | Ar–H | Aromatic protons [17] |
| | | 2.5482 | 3H | S | $-CH_3$ | Methyl group of 1,2,4-triazole moiety [18]. |

| | | | | | | |
|---|---|---|---|---|---|---|
| | TS | 12.249 | 1H | S | –OH | Hydroxyl proton of Salicylaldehyde moiety [19] |
| | | 10.688 | 1H | S | -SH | -SH proton of 1,2,4-triazole moiety. |
| | | 8.763 | 1H | S | -C=N- | Azomethine proton (Schiff base linkage) |
| | | 8.755-6.801 | 4H | M | Ar–H | Aromatic protons |
| | | 2.462 | 3H | S | $-CH_3$ | Methyl group of 1,2,4-triazole moiety. |
| | TV | 13.093 | 1H | S | –OH | Hydroxyl proton of Salicylaldehyde moiety |
| | | 8.228 | 1H | S | -C=N- | Azomethine proton (Schiff base linkage) |
| | | 7.806-6.711 | 4H | M | Ar–H | Aromatic protons |
| | | 3.000-2.977 | 1H | M | $–OCH_3$ | Methoxy group of O-vanillin moiety |
| | | 2.470 | 3H | S | $-CH_3$ | Methyl group of 1,2,4-triazole moiety. |
| $^{13}C$ | TC | 157.125 | 1C | — | C-SH | Nibouring carbon atom of the -SH moiety [20] |
| | | 149.177 | 1C | — | –C=N- | Azomethine carbon (Schiff base linkage) |
| | | 141.689 | 1C | — | $-C-CH_3$ | Carbon adjacent to methyl group [21] |
| | | 138.312 | 1C | — | C–OH | Carbon adjacent to benzene in cinnamaldehyde moiety |
| | | 130.211-116.681 | 8C | — | Ar–C | Aromatic carbons |
| | | 12.109 | 1C | — | $–CH_3$ | Methyl carbon of O-1,2,4-triazole moiety. |
| | TS | 161.652 | 1C | — | C-SH | Nibouring carbon atom of the -SH moiety |
| | | 160.824 | 1C | — | C–OH | hydroxyl group in Salicylaldehyde moiety [22] |
| | | 155.333 | 1C | — | –C=N- | Azomethine carbon (Schiff base linkage) |
| | | 154.045 | 1C | — | $-C-CH_3$ | Carbon adjacent to methyl group |
| | | 127.106-102.683 | 4C | — | Ar–C | Aromatic carbons |
| | | 18.624 | 1C | — | $–CH_3$ | Methyl carbon of O-1,2,4-triazole moiety. |

| | | | | | |
|---|---|---|---|---|---|
| TV | 160.426 | 1C | — | C-SH | Nibouring carbon atom of the -SH moiety |
| | 158.802 | 1C | — | C–OH | hydroxyl group in Salicylaldehyde moiety |
| | 153.475 | 1C | — | –C=N- | Azomethine carbon (Schiff base linkage) |
| | 148.205 | 1C | — | -C-$CH_3$ | Carbon adjacent to methyl group |
| | 132.980-96.311 | 4C | — | Ar–C | Aromatic carbons |
| | 30.706 | 1C | — | –$OCH_3$ | Methoxy carbon of Vanillin moiety |
| | 12.866 | 1C | — | –$CH_3$ | Methyl carbon of O-1,2,4-triazole moiety. |

*3.1.2. FT-IR Analysis*

In FT-IR spectra of synthesized Schiff base ligands were analysed in the range 4000–400 $cm^{-1}$ on a Bruker Alpha-T FT-IR spectrophotometer by making the KBr pellets. The observed functional group data will have depicted in the Table-2 and showed in the supplementary materials S7-S9, will confirms the formation of the Schiff base ligand.

**Table-2:** FT-IR spectral data of Schiff base ligands (TC, TS, TV).

| Wavenumber ($cm^{-1}$) | Assignment | Ligand(s) |
|---|---|---|
| 3419.47, 3422.68 | O–H stretching (Salicylaldehyde, Vanillin moiety) [23] | TC, TV |
| 3402.78 | O–H stretching (coordinated water) [24] | TC |
| 2920.51, 2930.14, 2940.42 | S–H stretching (Triazole moiety) [25] | TC, TS, TV |
| 1584.15, 1613.05, 1585.15 | C=N stretching (azomethine group, Schiff base formation) [26] | TC, TS, TV |
| 1176.38, 1126.29 | N–N stretching [27] | TC, TS, TV |

*3.1.3. LC-MS Spectral Analysis.*

LCMS analysis obtained molecular ion peaks at *m+1* 245.3182, 235.9995, and 265.2245 for the Schiff base ligands, matching their calculated molecular weights. The data confirm the formation of Schiff base ligands. The LCMS molecular ions peaks were showed in Supplementary Information S10-S12.

*3.1.4. UV-Vis Spectral analysis*

Using a Shimadzu model 1650 double-beam spectrophotometer at room temperature, the UV-Visible absorption spectra of the synthesised compounds were recorded across the 200-800 nm range with DMF as the solvent. The absorbance values are showed in **Table-3** and it is Depicted in **Fig-1**. A range of solvents with different polarities—ethanol, methanol, DMF, and DMSO—were employed for the UV–Visible spectroscopic studies presented in **Fig. 1**. Schiff base ligands TC, TS, and TV show clear solvatochromic behaviour in their UV-Vis absorption spectra recorded in these solvents, which vary significantly depending on the solvent [28]. Each ligand displays two distinct absorption bands corresponding to π→π* and n→π* electronic transitions associated with the azomethine (–CH=N–) group and aromatic rings. The π→π* transitions in the aromatic system are responsible for the high-energy bands seen in the 280-330 nm region [29], while the n→π* transitions involving the imine nitrogen and the conjugated π-system are the source of the lower-energy bands in the 350-420 nm range. [30]. As a result of solvent-solute interactions and intramolecular charge transfer (ICT), excited states are stabilised more effectively in more polar solvents like DMSO and DMF, as indicated by a modest red shift in λmax and absorption intensity. When comparing TS to TC and TV, the ligand with the wider and stronger absorption bands indicates that there is more conjugation and electronic delocalisation in TS. Understanding the electronic transition behaviour of Schiff base ligands is crucial for chemosensing and metal-ion coordination applications; our results show how solvent polarity and molecular structure significantly impact this behaviour.

**Table-3:** UV–Visible absorption bands of Schiff base ligands and their metal ions.

| System | Wavelength (nm) | Assignment |
|---|---|---|
| TC (free ligand) | 273.24 | π–π* transition (intra-ligand)[28] |
| | 362.72 | n → π* transition (–C=N–) [28] |
| TC–$Cu^{2+}$ | 453.32 | LMCT [29] |
| TC–$Fe^{2+}$ | 443.82 | LMCT [30] |
| TC–$Pb^{2+}$ | 442.64 | LMCT [31] |
| TS (free ligand) | 246.67 | π–π* transition (intra-ligand) |
| TS (free ligand) | 370.29 | n → π* transition (–C=N–) |

| | | |
|---|---|---|
| TS–$Cu^{2+}$ | 449.19 | LMCT |
| TS–$Fe^{2+}$ | 440.00 | LMCT |
| TS–$Pb^{2+}$ | 359.09 | LMCT |
| TV (free ligand) | 279.61 | π–π* transition (intra-ligand) |
| TV (free ligand) | 437.73 | n → π* transition (–C=N–) |
| TV–$Cu^{2+}$ | 619.72 | d–d transition |
| TV–$Fe^{2+}$ | 540.17 | d–d transition |
| TV–$Pb^{2+}$ | 495.58 | d–d transition |

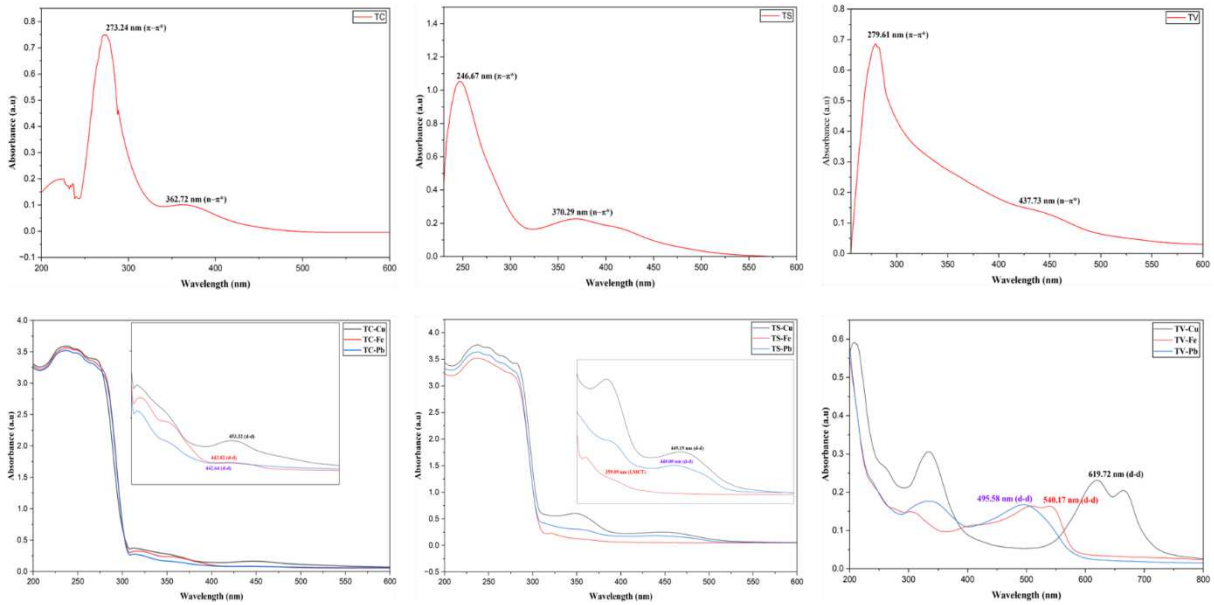


**Fig-2:** UV-visible spectra of the Schiff base ligands & its metal ions.

*3.2. Computational studies.*

*3.2.1. Density Functional Theory (DFT) analysis.*

DFT analysis is carried out to understand the physicochemical properties of TC, TS & TV. Parameters derived from DFT, including dipole moment, softness and hardness, electrophilicity indices, electronegativity and HOMO-LUMO energy gap of synthesized complexes are computed [32]. The optimized structure of these molecules is presented in **Fig-3** (TC, TS & TV).

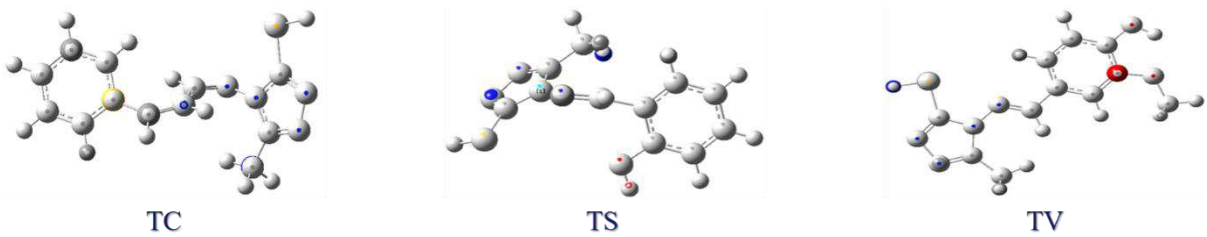


**Fig-3:** Optimized Structure of Schiff Base ligands.

The DFT-based descriptors were evaluated by applying Koopmans's approximation to the calculated frontier orbital energies, [33] which are as under:

$$I_P = -\epsilon_{HOMO} \quad (1)$$

$$E_A = -\epsilon_{LUMO} \quad (2)$$

Where, $E_A$ and $I_P$ are the Electron Affinity and Ionization Potential of these systems respectively.

Based on Eqn. (1) and (2), molecular hardness, softness, electronegativity, and electrophilicity index of these compounds are calculated as:

$$Molecular\ Hardness, \eta = \frac{I-A}{2} \quad (3)$$

$$Softness, S = \frac{1}{2\eta} \quad (4)$$

Table-4 lists the computational density function theory-based descriptors of the Schiff base ligands (TC, TS, & TV). The energy gap between the HOMO and LUMO transitions is a crucial parameter for understanding the electronic properties of any chemical species [34]. It is widely recognized that molecules exhibiting a larger HOMO–LUMO energy gap possess greater thermodynamic stability, whereas those with a smaller gap are typically more chemically reactive. As indicated in Table-4, the HOMO-LUMO gap of TC, TS, & TV are determined to be 3.8822, 4.4869, & 4.1524 eV respectively. This suggests that all three synthesized molecules exhibit considerable stability. The spatial distribution and electronic nature of the frontier molecular orbitals (HOMO and LUMO) for the synthesized compounds are depicted in **Fig-4**, providing further insight into their electronic structures.

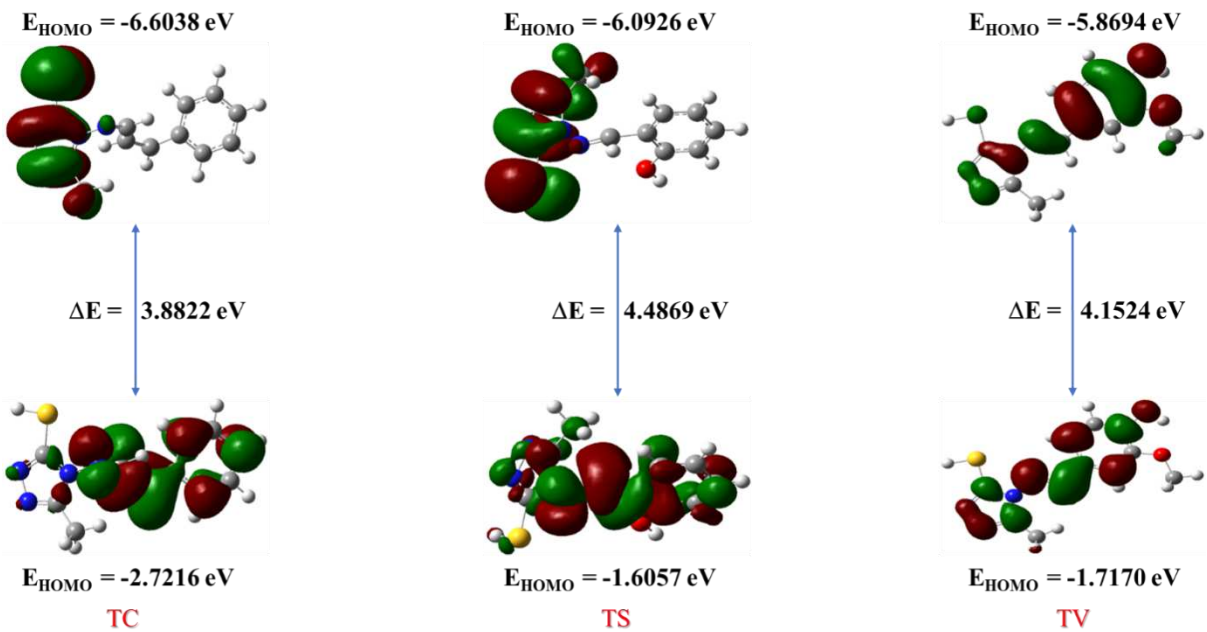

**Fig-4:** Frontier molecular orbital (HOMO-LUMO) of the Schiff base ligand (TC, TS, & TV).

**Table-4:** CDFT-based descriptors of Schiff base ligands (TC, TS, & TV).

| Species | $E_{HOMO}$ (eV) | $E_{LUMO}$ (eV) | $E_G$ (eV) | Hardness (eV) | Softness ($eV^{-1}$) | Dipole moment (Debye) |
|---|---|---|---|---|---|---|
| TC | -6.6038 | -2.7216 | 3.8822 | 0.071295 | 7.0131 | 13.9562 |
| TS | -6.0926 | -1.6057 | 4.4869 | 0.08249 | 6.0613 | 6.6323 |
| TV | -5.8694 | -1.7170 | 4.1524 | 0.076275 | 6.5552 | 8.0835 |

### *3.3. Visual identification of metal ions*

In an aqueous solution (1:1), the synthesized Schiff base ligands' selectivity towards the various metal ions ($Cu^{2+}$, $Fe^{2+}$, and $Pb^{2+}$) was examined. As seen in Fig-5, distinct and noticeable colour changes were seen upon complexation. Every ligand showed a distinct reaction to certain metal ions: in the presence of $Cu^{2+}$, $Fe^{2+}$, and $Pb^{2+}$, respectively, TS, TC, and TV showed strong selectivity along with dramatic colour changes. Table-5 provides a summary of the observed colour changes that correspond to ligand–metal interactions.

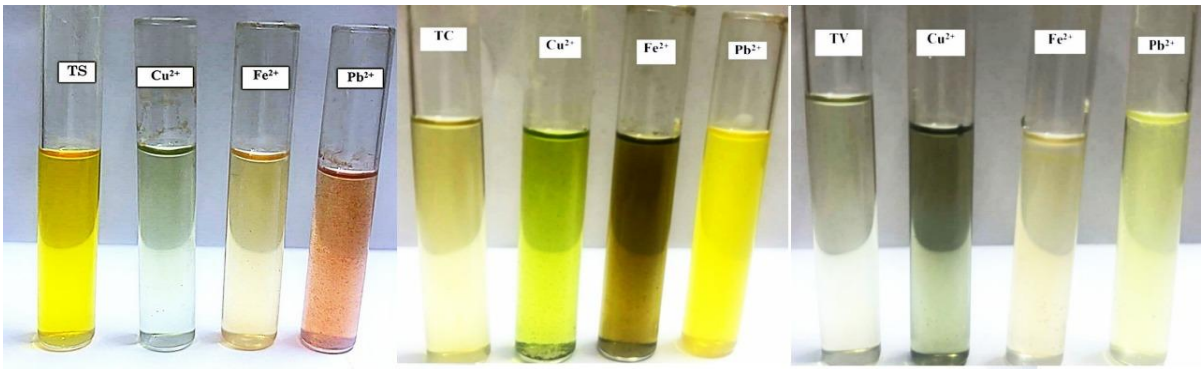


**Fig-5:** Naked Eye Color change of SB ($1x10^{-2}$ M in DMF) before and after the addition of metal ions ($1x10^{-2}$ M in $H_2O$) ions respectively.

**Table-5**. Visual detection of metal ions from synthesized ligands.

| Species | $Cu^{2+}$ | $Fe^{2+}$ | $Pb^{2+}$ |
|---|---|---|---|
| TS | orange to green | Orange to light yellow | orange to red |
| TC | Light Yellow to light green | Light Yellow to dark green | Light Yellow to dark yellow |
| TV | Light green to dark green | Light green to light pink | Light green to yellow. |

### *3.4. Stoichiometry of ligands-metal ion binding*

The complexation stoichiometry between the ligands (TS, TC, and TV) and the metal ions ($Cu^{2+}$, $Pb^{2+}$, and $Fe^{2+}$) was determined using Job's method of continuous variation. In this

procedure, the total concentration of ligand–metal mixtures were kept constant while varying their mole fractions. The absorbance values, recorded at the respective λ-max of each complex, were plotted against the mole fraction of the ligand. The resulting Job's plots clearly indicated a ligand-to-metal binding ratio of 1:1 for all the investigated complexes.

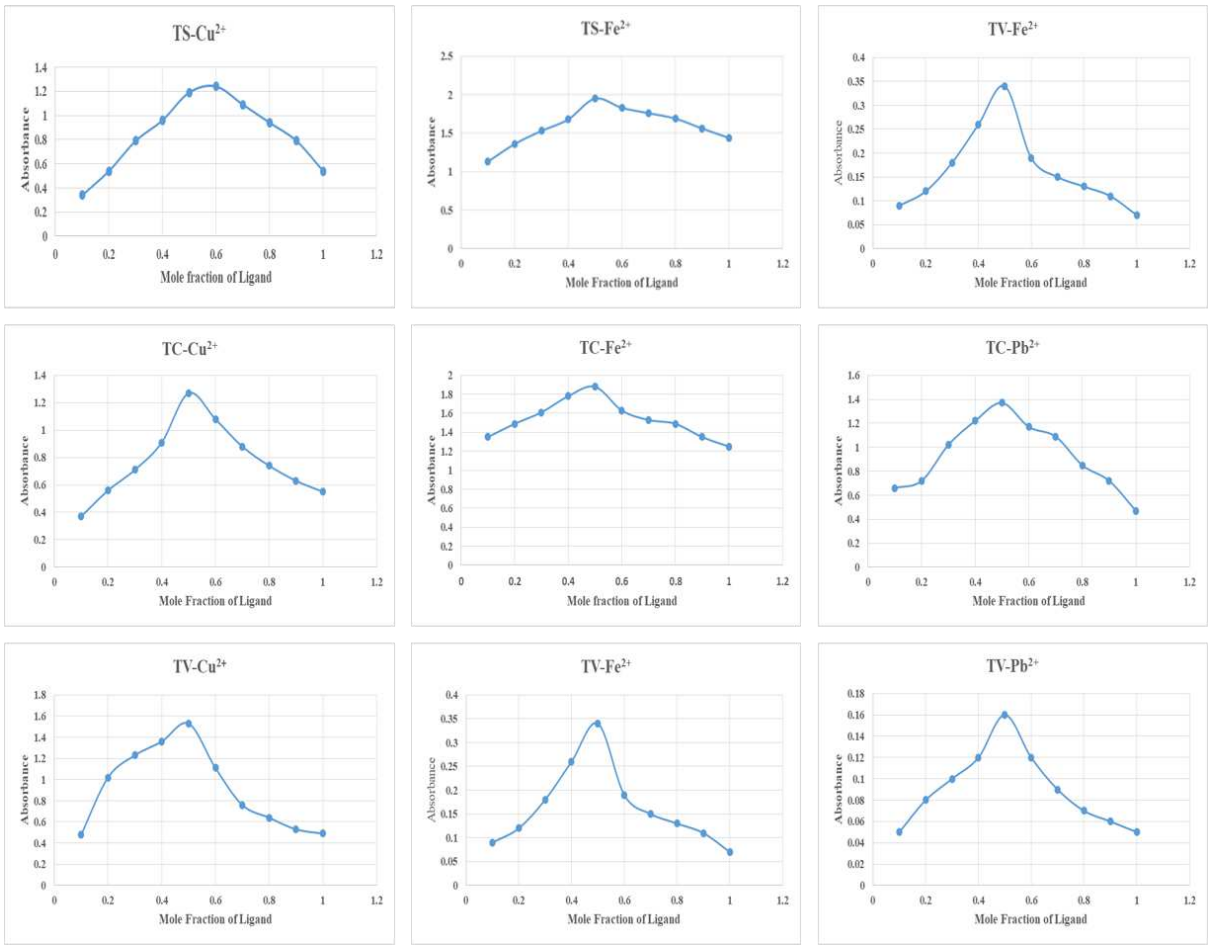


**Fig-6**: Jobs Plot demonstrating binding stoichiometry amongst metals and ligands

To explore the sensitivity, and binding mechanism of $Cu^{2+}$, $Pb^{2+}$ and $Fe^{2+}$ metal ions with the ligands in forming metal complexes and utilize the continuous variation method, employing Job's plot was showed in Fig-6. This is a well-known and continuous process for determining a complex's stoichiometric ratio an Equimolar mixture of metal ions (1 x $10^{-2}$ M) and ligands (1 x $10^{-2}$ M) is prepared, resulting in a series of solutions with the same total concentration of metal and ligand, each with a volume of 10 mL, but varying concentrations of metal and ligand individually [35]. The absorbance of solutions with different concentrations are measured and plotted against the mole fraction of the ligand.

*3.4.1. Electronic absorption Spectroscopic Titration.*

We conducted UV-Visible titration studies in DMF to study the binding behaviour and sensitivity of $Fe^{2+}$, $Pb^{2+}$, and $Cu^{2+}$ ions to the Schiff base ligands (TC, TS, and TV). As illustrated in Figure 7, the ligands' absorption spectra change as metal ions are added incrementally. As the concentration of metal ions rose, the absorbance gradually increased, with distinct isosbestic points at 443 nm ($Fe^{2+}$), 442 nm ($Pb^{2+}$), and 453 nm ($Cu^{2+}$) for TC, 359 nm ($Fe^{2+}$), 440 nm ($Pb^{2+}$), and 449 nm ($Cu^{2+}$) for TS, and 540 nm ($Fe^{2+}$), 495 nm ($Pb^{2+}$), and 619 nm ($Cu^{2+}$) for TV, as shown in Table-6.

Based on the calibration plots showing the relationship between absorbance and concentration, the detection limits for all three metal ions were found to be $1.2 \times 10^{-}5$ M. The results show that the ligands can recognise $Cu^{2+}$, $Fe^{2+}$, and $Pb^{2+}$ ions selectively at micromolar concentrations, and they work well at concentrations up to $10^{-2}$M. In keeping with the bidentate nature of these Schiff base ligands and their capacity to stabilise metal complexes, the observed binding mechanism is most likely coordinated with the azomethine nitrogen atom.

Mass spectrometric analysis was performed on the Schiff base complexes attached to metal ions to provide further support for these findings. A 1:1 ligand-to-metal stoichiometry was confirmed by the spectra, which showed molecular ion peaks, thereby validating the suggested binding relationship.

**Table-6:** UV–Vis isosbestic points and detection limits of Schiff base ligands with metal ions

| Ligand | Metal Ion | Isosbestic Point (nm) | Detection Limit (M) |
|---|---|---|---|
| **TC** | $Fe^{2+}$ | 443 | $1.2 \times 10^{-5}$ |
| | $Pb^{2+}$ | 442 | $1.2 \times 10^{-5}$ |
| | $Cu^{2+}$ | 453 | $1.2 \times 10^{-5}$ |
| **TS** | $Fe^{2+}$ | 359 | $1.2 \times 10^{-5}$ |
| | $Pb^{2+}$ | 440 | $1.2 \times 10^{-5}$ |
| | $Cu^{2+}$ | 449 | $1.2 \times 10^{-5}$ |
| **TV** | $Fe^{2+}$ | 540 | $1.2 \times 10^{-5}$ |
| | $Pb^{2+}$ | 495 | $1.2 \times 10^{-5}$ |
| | $Cu^{2+}$ | 619 | $1.2 \times 10^{-5}$ |

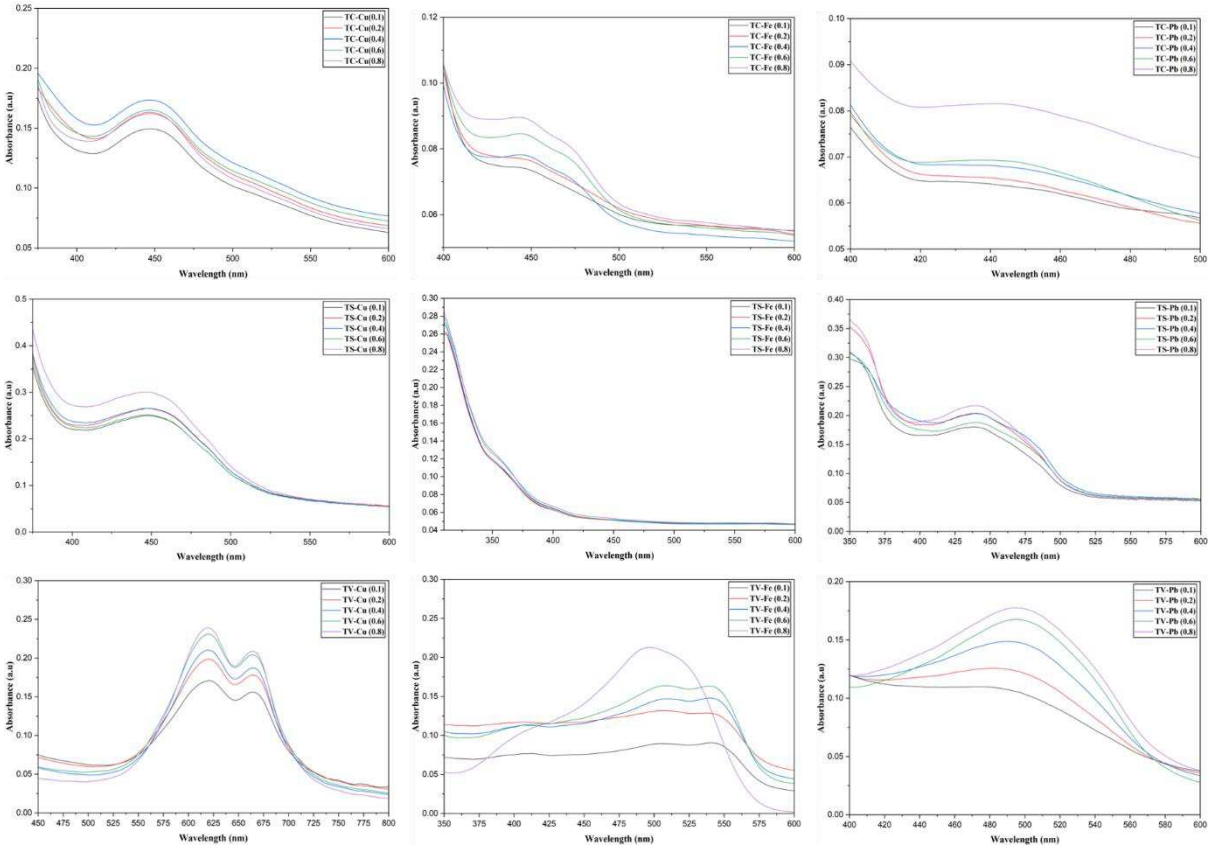


**Fig-7:** UV–Visible titration spectra of Schiff base ligands (TC, TS, and TV) with incremental addition of $Cu^{2+}$, $Fe^{2+}$, and $Pb^{2+}$ ions in DMF.

## 4. Conclusion:

To summarise, the azomethine functional groups found in the synthesised Schiff base ligands (TS, TC, and TV) show great promise as chemosensors for the selective detection of $Cu^{2+}$, $Fe^{2+}$, and $Pb^{2+}$ ions. Colorimetric studies conducted in a solution of $H_2O$ and ethanol allowed for the quick visual identification of individual metal ions by revealing clear and easily discernible changes in colour. The ligands' low limit of detection for $Cu^{2+}$, $Fe^{2+}$, and $Pb^{2+}$ was as low as $1.2 \times 10^{-2}$ M, proving their extreme sensitivity. The complexation mechanism was elucidated mechanistically by complementary CDFT investigations, which brought attention to the bidentate coordination mode through the imine nitrogen atoms. In addition, the experimental results were supported by Job's plot analysis, which demonstrated a ligand-to-metal stoichiometry of 1:1. All things considered, these findings demonstrate that the Schiff base ligands are highly selective and sensitive chemosensors, which bodes well for their potential use in analytical and environmental monitoring applications.

## Declaration of Competing Interest

The authors declare the following financial interests and/or personal relationships that may be perceived as potential competing interests: Chaitanya Lakshmi G acknowledges administrative support from Presidency University and discloses an employment affiliation with the institution.

## Conflicts of interest

The authors declare no conflicts of interest.

## Data availability

The data is available with corresponding author with request.

## References

[1] T. Rajan Arun, H. Phani Kumar, and S. Kamalesu, "Exploring the utilization of Schiff base metal complexes in biological settings: A review," *Inorganic Chemistry Communications*, vol. 170, p. 113251, 2024, doi: 10.1016/j.inoche.2024.113251.

[2] V. K. Juyal *et al*., "Schiff base metal complexes as a versatile catalyst: A review," *Journal of Organometallic Chemistry*, vol. 999, p. 122825, 2023, doi: 10.1016/j.jorganchem.2023.122825.

[3] M. Bheemarasetti *et al*., "Novel Schiff base metal complexes: Synthesis, characterization, DNA binding, DNA cleavage and molecular docking studies," *Journal of the Iranian Chemical Society*, vol. 15, no. 6, pp. 1377–1389, 2018, doi: 10.1007/s13738-018-1338-7.

[4] P. H. Amith Nayak, H. S. Bhojya Naik, H. B. Teja, B. R. Kirthan, and R. Viswanath, "Synthesis and opto-electronic properties of green light emitting metal Schiff base complexes," *Molecular Crystals and Liquid Crystals*, vol. 722, no. 1, pp. 67–75, 2021, doi: 10.1080/15421406.2020.1868053.

[5] A. A. Aly, E. M. Abdallah, S. A. Ahmed, M. M. Rabee, and S. Bräse, "Transition metal complexes of thiosemicarbazides, thiocarbohydrazides, and their corresponding carbazones with Cu(I), Cu(II), Co(II), Ni(II), Pd(II), and Ag(I)—A review," *Molecules*, vol. 28, no. 4, pp. 1–39, 2023, doi: 10.3390/molecules28041808.

[6] P. Singh, K. Kaur Sodhi, P. Yadav, A. Tomer, and S. Bali Mehta, "Advancement in the synthesis of metal complexes with special emphasis on Schiff base ligands and their important biological aspects," *Results in Chemistry*, vol. 7, p. 101222, 2024, doi: 10.1016/j.rechem.2023.101222.

[7] D. Dragancea *et al*., "Vanadium(V) complexes with substituted 1,5-bis(2-hydroxybenzaldehyde)carbohydrazones and their use as catalyst precursors in oxidation of

cyclohexane," *Inorganic Chemistry*, vol. 55, no. 18, pp. 9187–9203, 2016, doi: 10.1021/acs.inorgchem.6b01011.

[8] F. S. Al-Fartusie and S. N. Mohssan, "Essential trace elements and their vital roles in human body," *Indian Journal of Advances in Chemical Science*, vol. 5, no. 3, pp. 127–136, 2017, doi: 10.22607/IJACS.2017.503003.

[9] A. Ejigu, M. Tefera, and A. Guadie, "A review article on: Voltammetric detection of lead, mercury, chromium, and arsenic metal ions from environmental samples," *Electrochemistry Communications*, vol. 178, p. 107996, 2025, doi: 10.1016/j.elecom.2025.107996.

[10] P. Kaur, R. Kaur, and M. Goswami, "A review on methods of synthesis of 1,2,4-triazole derivatives," *International Research Journal of Pharmacy*, vol. 9, no. 7, pp. 1–35, 2018, doi: 10.7897/2230-8407.097121.

[11] S. N. Shariff, D. M. K. B., S. Ranganatha, S. Supriya, S. Rajendrachari, and D. Ramakrishna, "Unveiling optical nonlinearity: Exploring nickel-curcumin complexes through Z-scan and degenerate four-wave mixing techniques," *ChemistrySelect*, vol. 9, 2024, doi: 10.1002/slct.202401443.

[12] S. N. Shariff *et al*., "Zinc-curcumin complexes: Design, synthesis, geometry optimization, and optical nonlinearity applications," *Optical Materials*, vol. 143, p. 114164, 2023, doi: 10.1016/j.optmat.2023.114164.

[13] A. S. Ramasubramanian, B. Ramachandra Bhat, and R. Dileep, "Synthesis, characterization, and biological activity of metal complexes of 4-ethyl vanillideneamino-3-methyl-5-mercapto-1,2,4-triazole," *Journal of Coordination Chemistry*, vol. 63, no. 17, pp. 3108–3116, 2010, doi: 10.1080/00958972.2010.505283.

[14] N. Ashwini, R. Dileep, and S. Ranganatha, "Inhibition effect of eco-friendly curcumin based Schiff base on industrially important mild steel material corrosion: Electrochemical and quantum chemical evaluation," *Results in Surfaces and Interfaces*, vol. 18, p. 100457, 2025, doi: 10.1016/j.rsurfi.2025.100457.

[15] M. Fizer, M. Slivka, V. Sidey, V. Baumer, and O. Fizer, "On the protonation of a polysubstituted 1,2,4-triazole: A structural study of a hexabromotellurate salt," *Journal of Molecular Structure*, vol. 1241, p. 130632, 2021, doi: 10.1016/j.molstruc.2021.130632.

[16] D. Ramakrishna, "Physicochemical and non-linear optical studies of mixed ligand Cu(I), Fe(II) and Ru(II) complexes containing triphenylphosphine and a Schiff base derived from furfural and hydrazine hydrate," *Chemical Data Collections*, vol. 28, p. 100424, 2020, doi: 10.1016/j.cdc.2020.100424.

[17] S. Shakeel Nawaz *et al*., "Nickel curcumin complexes: Physico chemical studies and nonlinear optical activity," *Optical Materials*, vol. 136, p. 113450, 2023, doi: 10.1016/j.optmat.2022.113450.

[18] A. Kashyap and O. Silakari, "Chapter 9—Triazoles: Multidimensional 5-membered nucleus for designing multitargeting agents," in *Key Heterocyclic Chemistry for Drug Discovery*, O. Silakari, Ed. Elsevier, 2018, pp. 323–342, doi: 10.1016/B978-0-08-102083-8.00009-1.

[19] M. Hoelm, J. Adamczyk, K. Wzgarda-Raj, and M. Palusiak, “Effect of a substituent on the properties of salicylaldehyde hydrazone derivatives,” *Journal of Organic Chemistry*, vol. 88, no. 4, pp. 2132–2139, 2023, doi: 10.1021/acs.joc.2c02547.

[20] A. Cassidy *et al*., “Patterned formation of enolate functional groups on the graphene basal plane,” *Physical Chemistry Chemical Physics*, vol. 20, no. 45, pp. 28370–28374, 2018, doi: 10.1039/C8CP05730C.

[21] V. Myrseth, K. J. Børve, and T. D. Thomas, “The substituent effect of the methyl group: Carbon 1s ionization energies, proton affinities, and reactivities of the methylbenzenes,” *Journal of Organic Chemistry*, vol. 72, no. 15, pp. 5715–5723, 2007, doi: 10.1021/jo0708902.

[22] V. K. Basappa Chidananda, D. Ramakrishna, M. Kaur, and R. Hosakere Doddarevanna, “Benzimidazolyl based Schiff base palladium complex in an ionic liquid: An effective combination for Suzuki coupling,” *Journal of Coordination Chemistry*, vol. 70, no. 9, pp. 1573–1584, 2017, doi: 10.1080/00958972.2017.1311412.

[23] S. N. Shariff, R. S., S. S., and R. Dileep, “Metal-centric organic compounds: Boon to third-order nonlinear optical applications,” *Reviews in Inorganic Chemistry*, vol. 44, 2023, doi: 10.1515/revic-2022-0038.

[24] S. N. Shariff, S. Saravu, and R. Dileep, “Schiff base complexes for catalytic application,” in *Catalysis—New Insights*, 2022, doi: 10.5772/intechopen.107904.

[25] F. Mohammadsaleh, M. D. Jahromi, A. R. Hajipour, S. M. Hosseini, and K. Niknam, “1,2,3-Triazole framework: A strategic structure for C–H···X hydrogen bonding and practical design of an effective Pd-catalyst for carbonylation and carbon-carbon bond formation,” *RSC Advances*, vol. 11, no. 34, pp. 20812–20823, 2021, doi: 10.1039/D1RA03356E.

[26] F. H. Suydam, “The C=N stretching frequency in azomethines,” *Analytical Chemistry*, vol. 35, no. 2, pp. 193–195, 1963, doi: 10.1021/ac60195a024.

[27] I. Gulaczyk, M. Kręglewski, and A. Valentin, “The N–N stretching band of hydrazine,” *Journal of Molecular Spectroscopy*, vol. 220, no. 1, pp. 132–136, 2003, doi: 10.1016/S0022-2852(03)00106-1.

[28] K. Choroba, J. Palion-Gazda, M. Penkala, and P. Rawicka, “Tunability of triplet excited states and photophysical behaviour of bis-cyclometalated iridium(III) complexes with imidazo[4,5-f][1,10]phenanthroline,” *Dalton Transactions*, 2024, supplementary information.

[29] S. D. Hebbar and D. R. Trivedi, “Discriminative ion detection of $Hg^{2+}$ and $Cu^{2+}$ and selective recognition of $PO_4^{3-}$ ions: Real-time monitoring in food and water samples and molecular keypad lock integration,” *Spectrochimica Acta Part A: Molecular and Biomolecular Spectroscopy*, vol. 331, p. 125706, 2025, doi: 10.1016/j.saa.2025.125706.

[30] P. Mendu, C. G. Kumari, and R. Ragi, “Synthesis, characterization, DNA binding, DNA cleavage and antimicrobial studies of Schiff base ligand and its metal complexes,” *Journal of Fluorescence*, vol. 25, no. 2, pp. 369–378, 2015, doi: 10.1007/s10895-015-1520-6.

[31] N. G. Yernale and M. Bennikallu Hire Mathada, “Synthesis, characterization, antimicrobial, DNA cleavage, and *in vitro* cytotoxic studies of some metal complexes of Schiff base ligand derived from thiazole and quinoline moiety,” *Bioinorganic Chemistry and Applications*, vol. 2014, 2014, doi: 10.1155/2014/314963.

[32] H. B. V. Sowmya *et al*., “Solvent free synthesis, crystal studies, docking studies and antibacterial properties of some novel fluorinated pyridazinone derivatives,” *Journal of Molecular Structure*, vols. 1054–1055, pp. 179–187, 2013, doi: 10.1016/j.molstruc.2013.09.046.

[33] R. Vargas, J. Garza, and A. Cedillo, “Koopmans-like approximation in the Kohn–Sham method and the impact of the frozen core approximation on the computation of the reactivity parameters of the density functional theory,” *Journal of Physical Chemistry A*, vol. 109, no. 39, pp. 8880–8892, 2005, doi: 10.1021/jp052111w.

[34] V. Hadigheh Rezvan, “Molecular structure, HOMO–LUMO, and NLO studies of some quinoxaline 1,4-dioxide derivatives: Computational (HF and DFT) analysis,” *Results in Chemistry*, vol. 7, p. 101437, 2024, doi: 10.1016/j.rechem.2024.101437.

[35] P. Duenas-Ramirez *et al*., “Highly chelating stellate mesoporous silica nanoparticles for specific iron removal from biological media,” *Journal of Colloid and Interface Science*, vol. 579, pp. 140–151, 2020, doi: 10.1016/j.jcis.2020.06.013.

## Supplementary Files

This is a list of supplementary files associated with this preprint. Click to download.

- SupplementaryInformationseries206092026.docx